ELSEVIER

Computers in Biology and Medicine 38 (2008) 713–726

Computers in Biology and Medicine

www.intl.elsevierhealth.com/journals/cobm

Optimising nasal spray parameters for efficient drug delivery using computational fluid dynamics

K. Inthavong[a], Z.F. Tian[a], J.Y. Tu[a,*], W. Yang[b], C. Xue[c]

[a]*School of Aerospace, Mechanical and Manufacturing Engineering, RMIT University, PO Box 71, Bundoora Vic 3083, Australia*
[b]*Division of Minerals, Commonwealth Scientific and Industrial Research Organization, PO Box 312, Clayton South Vic 3169, Australia*
[c]*School of Health Sciences, RMIT University, Australia*

Received 21 May 2007; accepted 24 March 2008

Abstract

Experimental images from particle/droplet image analyser (PDIA) and particle image velocimetry (PIV) imaging techniques of particle formation from a nasal spray device were taken to determine critical parameters for the study and design of effective nasal drug delivery devices. The critical parameters found were particle size, diameter of spray cone at a break-up length and a spray cone angle. A range of values for each of the parameters were ascertained through imaging analysis which were then transposed into initial particle boundary conditions for particle flow simulation within the nasal cavity by using Computational Fluid Dynamics software. An Eulerian–Lagrangian scheme was utilised to track mono-dispersed particles (10 and 20 μm) at a breathing rate of 10 L/min. The results from this qualitative study aim to assist the pharmaceutical industry to improve and help guide the design of nasal spray devices.

Keywords: Nasal spray; CFD; Nasal cavity; Numerical simulation; Particle deposition; Drug delivery

1. Introduction

Nasal drug delivery provides an alternative approach to traditional delivery methods such as oral drug routes that fail in the systemic delivery of compounds due to its dissociation by the digestive system. Additionally, it has a good level of patient compliance when compared with intravenous methods and produces faster pharmacological action. The nasal airway is dominated by the nasal turbinates; three bony, soft-tissue structures lined with highly vascularised mucosa that contain openings to the paranasal sinuses. Because of these characteristics, it is hypothesised that drug delivery to combat health problems such as lung diseases, cancers, diabetes, sinus infections, etc. may be viable if the drug formulation can be deposited in the turbinate region [1]. However, this requirement tends to be poorly implemented where a large proportion of the drug particles are known to deposit in the anterior regions of the nasal vestibule, attributed to the sprayed particles existing in a high inertial regime [2–4]. Therefore, studies into local particle deposition are of great significance in the delivery of drugs via the nasal airway. The knowledge of initial conditions from the atomised drug particles introduced into nasal cavity as well as the deposition mechanisms caused by the interaction of drug particles with the airflow field is required in order to develop optimised delivery devices (nasal sprays) and correct drug formulations.

The function of the delivery device is to atomise the liquid formulation into a fine spray made up of small micron-sized particles. Although the physics of sprays and atomisation has been studied quite extensively, the majority of the research has focussed on industrial applications, such as fuel injectors [5] and spray dryers [6], resulting in a lack of experimental data for nasal spray applications. Moreover, there exists a great difficulty in the ability to capture detailed measurements of the dense spray found at the near-nozzle region which has hindered the understanding of the atomisation process. Despite this, there have been numerous experimental studies

* Corresponding author. Tel.: +61 3 99256191; fax: +61 3 99256108.
E-mail addresses: s3113652@student.rmit.edu.au (K. Inthavong), zhaofeng.tian@rmit.edu.au (Z.F. Tian), jiyuan.tu@rmit.edu.au (J.Y. Tu), william.yang@csiro.com.au (W. Yang).

0010-4825/$ - see front matter © 2008 Elsevier Ltd. All rights reserved.
doi:10.1016/j.compbiomed.2008.03.008

Table 1
Variables related to the actuation of a nasal spray

Consumer variables	Parameter affected
Increased/decreased inhalation	Airflow rate
Nostrils opened (one or two)	Airflow pattern
Head tilt back/forward	Insertion angle inwards
Spraying away from septum walls	Insertion angle sideways
Strength of actuation	Particle size and velocity
Speed of actuation	Particle size and velocity
Insertion location	Surrounding geometry

documenting nasal particle deposition in the inertial regime by *in vivo* [7,8] as well as *in vitro* [3,4,9] methods. From these studies, deposition efficiencies were correlated with an inertial parameter that is a function of the flow rate, particle diameter and density. However, these studies investigated the natural inhalation of suspended particles from the surrounding air which was drawn into the nasal cavity through an extended pipe connected to the nares.

Nasal particle deposition delivered by a spray device was performed by Cheng et al. [10] using a multi-sectional nasal airway replica model and found deposition patterns from four different nasal spray pumps. The results showed the particles deposited mainly in the anterior and turbinate regions and that deposition in the anterior region increased with an increase in spray cone angles and larger particles. Suman et al. [11] investigated deposition patterns in relation to *in vitro* measurements of two different nasal spray pumps having different performance characteristics. It was found that spray characteristics, such as spray angle and plume geometry, did not affect the distribution of droplets in the nose. The discrepancy between the two correlations may be attributed to numerous variations that exist in nasal spray applications that are hard to quantify experimentally (Table 1). Furthermore, *in vivo* methods are not able to provide precise and detailed information regarding initial particle conditions and its relationship to the specific deposition site within the nasal passage.

An alternative approach to complement *in vivo* obtained data that lack precise details is to use computational techniques such as computational fluid dynamics (CFD). With the increase in computing power coupled with advances in numerical algorithms, CFD techniques have readily been used to examine critical information, such as the air velocity profile [12,13], particle trajectories and localised deposition sites [14,15]. However, these past studies focussed on the inhalation of suspended particles in the air. Therefore, this study aimed to investigate the capabilities and techniques of CFD to examine the effects of relevant spray device parameters, which were determined experimentally. Additionally, the influence that the spray parameters had on the deposition of particles within the nasal cavity was predicted and discussed. The scope of the experimental work solely aimed at providing a qualitative insight to determine what parameters exist in the atomisation of drug formulations from a nasal spray device; thus, a full quantitative analysis of the spray dynamics was left for a future report. The preliminary results were used to provide numerical initial boundary conditions for the inlet-sprayed particles and it is expected that these results will assist in future for a fully deterministic understanding of nasal spray atomisation. Moreover, the final computational results may be used to complement current data relating to nasal spray performance to assist the pharmaceutical industry in the design of an optimised nasal spray device.

2. Experimental and numerical methods

2.1. Experimental apparatus

The experimental setup employed for this study is shown in Fig. 1 which includes a test chamber, a pressurised water supply system, a liquid collection system and a visualization system. The test chamber was constructed of clear perspex box enclosing the spray nozzle that pointed downwards. Water was stored in a pressure tank and was fitted with a pressure line that had an allowable maximum operating pressure of 600 kPa at one end and a pressure regulator fitted at the outlet end. The maximum pressure was applied at the upstream and a pressure regulator was used to monitor a constant pressure in the system. The pressure at the spray nozzle would be slightly smaller than the reading at the regulator due to head losses; however, this was not significant as the primary aim was to obtain qualitative images.

Two visualization systems were employed: (i) a particle/droplet image analyser (PDIA) which enables detailed imaging of the spray and the formation of droplets and (ii) particle image velocimetry (PIV) which will provide an approximate velocity field. An ILA 2D PIV system was used, consisting of a SensiCam 12-bit digital CCD camera (1280 × 1024 pixels), which was synchronised with a New Wave 120 mJ double-cavity Nd:YAG Laser. In the PIV measurement, 800 pairs of successive images were taken at the laser repetition rate of 4 Hz. Hence, a mean velocity flow pattern was obtained by statistically averaging 800 successive instantaneous velocity vector maps over approximately 3 min.

For capturing of the spray, an Oxford Laser PDIA system was used. The CCD camera was situated approximately 10 cm from the test chamber which was dependent on the camera focal length. A long distance microscope lens provided a magnification of 2.46, offering a resolution of approximately 3.01 μm/pixel. Thus, each image, at 1280 × 1024 pixel resolution, was only able to capture a physical region of 3.85 mm × 3.08 mm. The camera was mounted on a traversing unit which allowed precise movements in all three coordinates to reposition the camera in order to capture the spray in full. A constant upstream pressure of 600 kPa was applied and the water was released through a pressure regulator valve and allowed to reach steady conditions before the images were taken. A single run was limited to approximately 3 min in order to avoid pressure variations associated with a decreasing liquid volume within the pressure tank. The spray nozzle used in this study was a nasal spray device kindly provided by Saint-Gobain/Calmar, Product Number 43110-016.

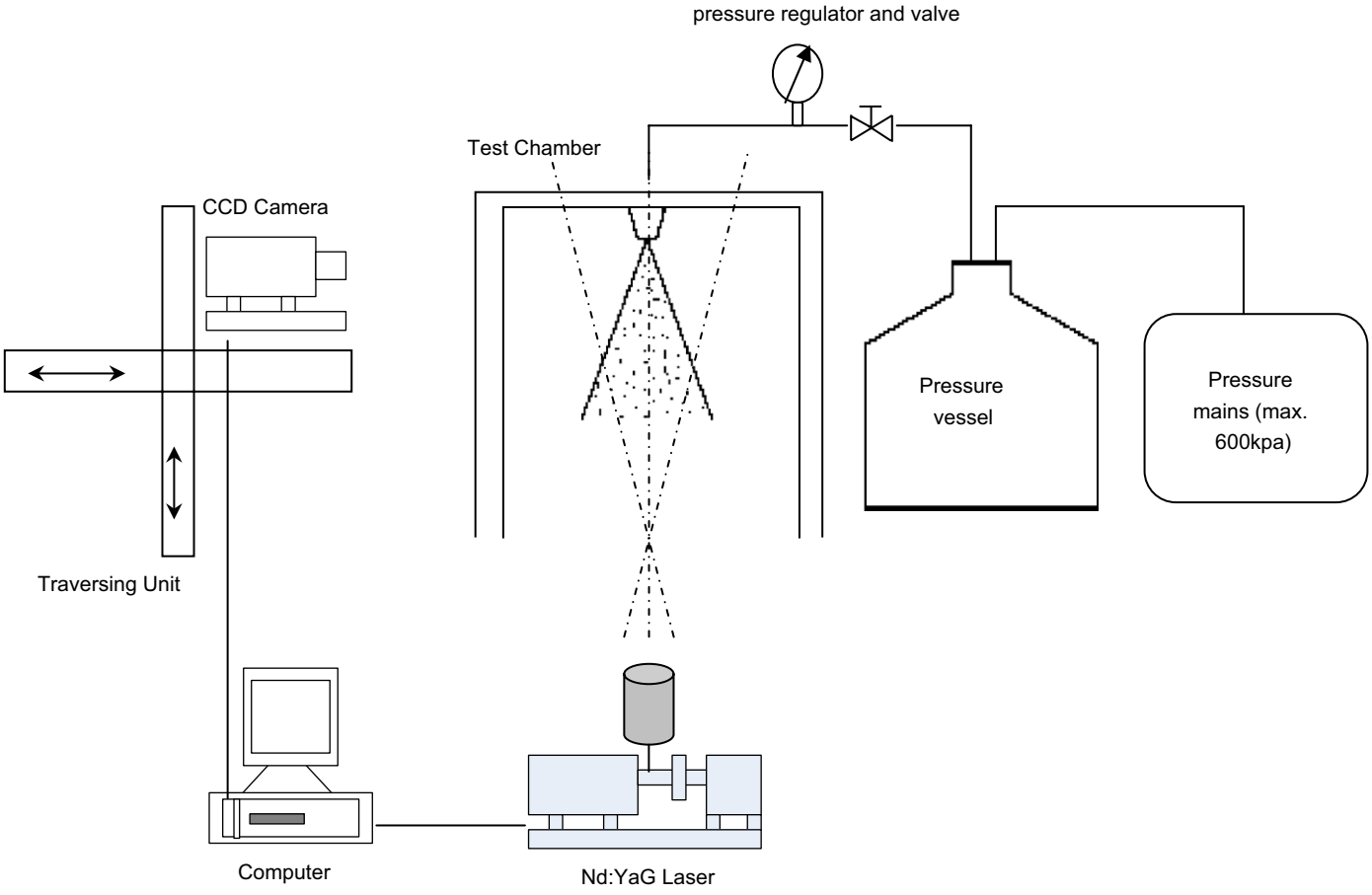

Fig. 1. Schematic of the experimental setup for spray visualization.

2.2. Nasal cavity geometry and grid generation

A nasal cavity geometry was obtained through a computed tomography (CT) scan of the nose of a healthy 25-year-old, Asian male (170 cm height, 75 kg mass). The reconstruction of the nasal cavity for the study of airflow and particle deposition in the literature has traditionally been performed using CT scans [14,16–19]. CT scans are useful as they have the ability to visualise bone structure directly which MRI scans do not do well. However, MRI scans are also used as they are better for imaging mucosal structures that are important factors in nasal patency and volume [20,21]. The CT scan was performed using a CTI whole body scanner (General Electric). The single-matrix scanner was used in helical mode with 1-mm collimation, a 40-cm field of view, 120 kV peak and 200 mA. The scans captured outlined slices in the *X–Y* plane at different positions along the *Z*-axis from the entrance of the nasal cavity to just anterior of the larynx at intervals of 1–5 mm depending on the complexity of the anatomy. The coronal-sectioned scans were imported into a 3D modelling program called GAMBIT which created smooth curves that connected points on the coronal sections. Surfaces were then created and stitched up to create a computational mesh. An initial model with 82,000 cells was created initially and used to solve the airflow field at a flow rate of 10 L/min. The original model was refined by cell adaptation techniques that included refining large volume cells that displayed high velocity gradients and near wall refinements. This process was repeated twice, with each repeat producing a model with a higher cell count than the previous model. Subsequently, four models were produced: 82,000, 586,000, 950,000 and 1.44 million cells. A model containing 950,000 cells is shown in Fig. 2 with three coronary slices showing the internal mesh with a dense region near the walls. A grid independence test found the results for average velocity taken along lines A and B converge around 950,000 cells (Fig. 3).

2.3. Gas phase modelling

Due to the complex geometry of the anatomically real nasal cavity a commercial CFD code, FLUENT was utilised to predict the continuum gas phase flow under steady-state conditions through solutions of the conservation equations of mass and momentum. These equations were discretised using the finite volume approach. The third-order accurate QUICK scheme was used to approximate the momentum equation while the pressure–velocity coupling was realized through the SIMPLE method. Flow rates of 5, 7.5, 10 and 15 L/min were used to simulate the range of adult breathing under a resting condition. At a flow rate of 15 L/min it was first determined by Swift and Proctor [22] that a laminar flow regime

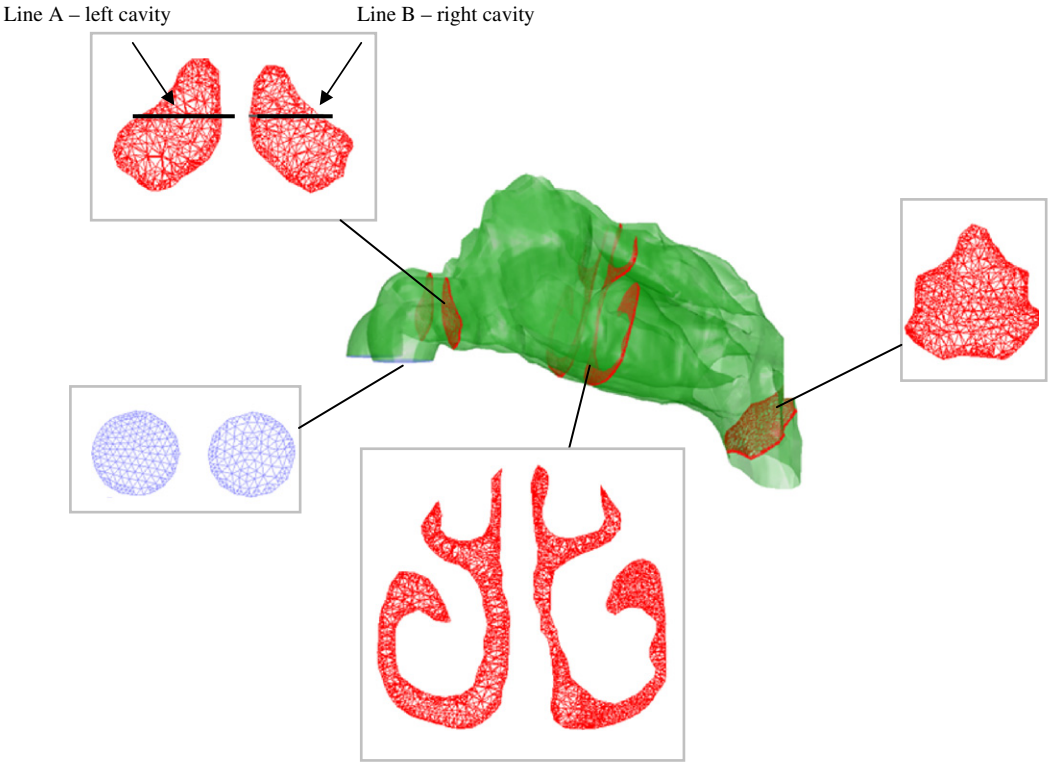

Fig. 2. Mesh resolution for 950,000 cell model. Three coronary sections aree displayed and lines A and B are taken in the spanwise direction at the nasal valve region.

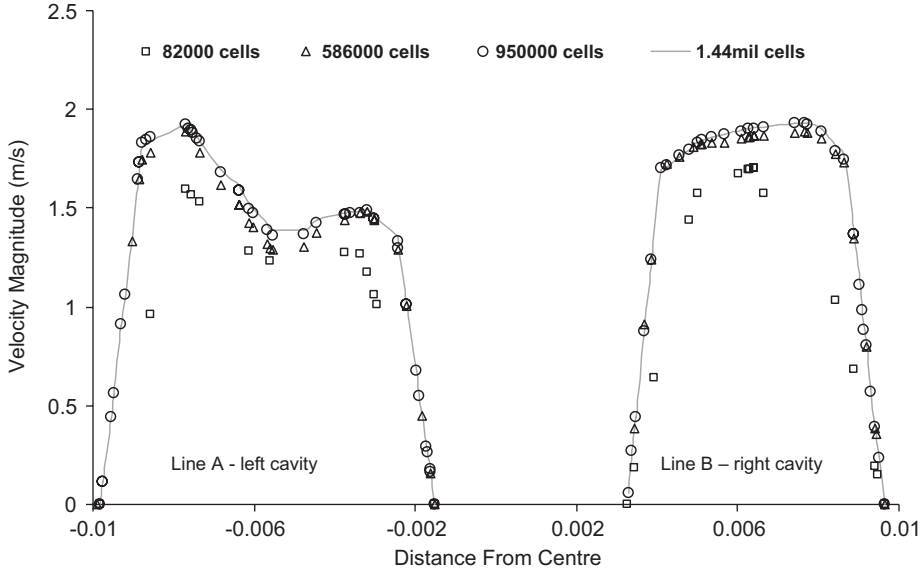

Fig. 3. Grid independence test based on a velocity profile taken at the contracting nasal valve region of both cavities.

persisted through the main nasal passage while for a flow rate of 25 L/min a transition to turbulence occurred downstream of the nasal valve. Hahn et al. [23] using PIV measurements on a scaled-up model reported a predominantly laminar flow for a breathing rate of 15 L/min while a flow rate of 33 L/min was considered moderately turbulent. The nature of the flow is often characterised by the dimensionless value called the Reynolds number (*Re*), which is the ratio of inertia to viscous forces:

$$Re = \frac{\rho_g u D}{\mu_g} \tag{1}$$

where ρ_g = gas density, μ_g = gas viscosity, U = gas velocity and L = a characteristic length. Taking the inlet nostril diameter as the characteristic length the calculated *Re* for the nasal cavity at 15 L/min is 1000 while for straight internal pipe flows a

laminar flow regime exists for $Re < 2000$. The nasal cavity with its convoluted narrow passageways will always exhibit disruptions to the flow causing regions that exhibit turbulent flow characteristics such as flow separation and recirculation despite the low velocities. The strength and the significance of these disruptions to the overall flow field are dampened as the velocity decreases allowing the fluid viscosity to dominate. This study considered the multiphase (gas and particle) flow to be in a laminar flow regime similar to past simulations which have successfully implemented a laminar flow for similar airflow rates [13,14,24,25]. This was deemed appropriate as the flow disturbances occurring within the passageways will have a small effect on the overall flow field due to the low velocities being dampened by viscous forces.

A steady flow rather than a cyclic unsteady flow was used in this case to allow the results to emphasize the airflow dynamics and patterns independent from cyclic conditions. Moreover, the significance of the fluctuating sinusoidal pattern of the inhalation–exhalation breathing cycle on the nasal airflow can be estimated by examining the Womersley number, α, and the Strouhal number, S. The calculated Womersley number

$$\alpha = \frac{D}{2}\sqrt{\frac{\omega}{\nu_g}} \tag{2}$$

was 1.68 while the Strouhal number

$$S = \frac{\omega D}{u_{ave}} \tag{3}$$

was 0.01. D is equal to 0.01 m and is the characteristic length which was taken as the average hydraulic diameter of 30 cross-sections taken throughout the nasal cavity. ν_g is the kinematic viscosity of air and ω is the breathing frequency equal to $\omega = 2\pi f = 1.57/s$ and u_{ave} is the average velocity through the nasal passage under the flow rate of 15 L/min which is equal to 0.9 m/s. Although the Womersley number is greater than 1, it is not much greater; while the low value for S suggests that the flow may be assumed to be quasi-steady. It has, however, been shown experimentally that the oscillatory effects are not present until $\alpha \geqslant 4$ [16]. Additionally, other studies have also concluded that under most conditions especially low flow rates, the nasal airflow can be considered quasi-steady [23,26,27]. The steady-state continuity and momentum equations for the gas phase (air) in Cartesian tensor notation are

$$\frac{\partial}{\partial x_i}(\rho_g u_i^g) = 0 \tag{4}$$

$$\rho_g u_j^g \frac{\partial u_i^g}{\partial x_j} = -\frac{\partial p_g}{\partial x_i} + \frac{\partial}{\partial x_j}\left(\mu_g \frac{\partial u_i^g}{\partial x_j}\right) \tag{5}$$

where u_i^g is the ith component of the time-averaged velocity vector and ρ_g is the air density.

2.4. Particle phase modelling

A Lagrangian particle tracking method is used to trace the dispersion of particles about the trajectory. The Lagrangian scheme is most popular in engineering applications for the prediction of particle flows because of its ability to track particles individually. Trajectories of individual particles can be tracked by integrating the force balance equations on the particle:

$$\frac{du_p}{dt} = F_D(u_g - u_p) + \frac{g(\rho_p - \rho_g)}{\rho_p} \tag{6}$$

where u_p is the particle velocity and ρ_p is the particle density. It is noted that the gravity term 'g' was taken as $-9.81\,m/s^2$ taken in the Y-axis and hence is applicable for an upright position.

Additional source terms for the particle equation such as Brownian force and Saffman lift force are not included as the particles concerned are substantially greater than submicron particles that are influenced by their mean free path. Additionally, the particles are far denser than air, causing terms that depend on the density ratio, such as the pressure force, buoyancy force, virtual mass effect and Basset force, to be very small [28]. The drag force per unit particle mass is $F_D(u_i^g - u_i^p)$ and F_D is given by

$$F_D = \frac{18\mu_g}{\rho_p d_p^2}\frac{C_D Re_p}{24} \tag{7}$$

where d_p is the particle volume equivalent diameter. u^p presents the particle velocity. μ_g is the molecular viscosity of the fluid. Re_p is the particle Reynolds number, which is defined as

$$Re_p \equiv \frac{\rho_p d_p |u_p - u_g|}{\mu_g} \tag{8}$$

2.5. Boundary conditions and assumptions

Although the atomisation of the drug formulation in a nasal spray produces a particle size distribution, mono-sized particles were used in this study to investigate the effects of particle size which is a dominant parameter when dealing deposition by inertial impaction. Two particle sizes were investigated, 10 μm for its low Stokes number characteristics and 50 μm which is typical of the mean particle size produced from nasal sprays [10]. Other approximations include isothermal flow and smooth, rigid, aerodynamic walls, which have been found to be sufficient [3] for parametrical studies. The wall boundary condition for the particles was set to 'trap', meaning that once the particle hits the wall it is trapped there and the effects of accretion and erosion of particles at the walls are not considered. A dilute void fraction for the spray was utilised; thus, one-way coupling was enabled and each particle was tracked individually and no particle–particle interactions, such as collisions and break-up that are more relevant to larger particles, occur.

3. Results and discussion

3.1. Spray characterisation

Fig. 4 shows two images of the spray that include (a) a single image at the near-nozzle region and (b) a portrait of the spray from the merging of all single images taken at different areas of the spray. It was observed that the pressure induced by the nasal spray actuation caused the liquid to emerge form

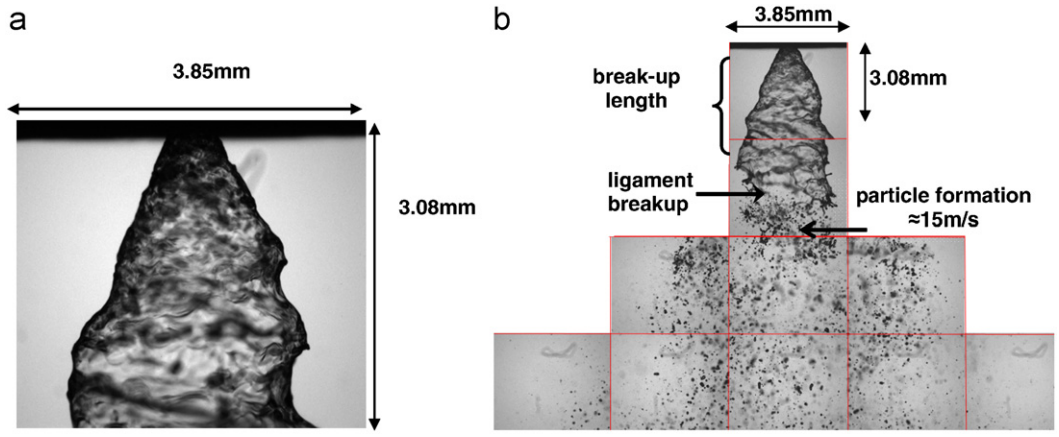

Fig. 4. (a) Single image at the near-nozzle region showing a swirling hollow sheet of liquid. (b) Collated image from the individual single images to create the entire spray field.

the orifice under the action of both radial and axial forces. A swirling thinning sheet of liquid was formed which was unstable, breaking up into ligaments before forming particles at a distance, called the break-up length, from the nozzle (Fig. 4b). A hollow spray cone was produced at the break-up length with the majority of particles located at the periphery of the hollow cone. This atomisation process is typically found through the use of pressure-swirl-type atomisers that are contained within the spray nozzle. Theory of pressure-swirl atomisation has been studied extensively for the last century with the vast majority of literature focussed on high pressure applications, such as fuel injectors found in the automotive industry. Although little has been researched on nasal spray applications it is evident that the key parameters that may influence nasal drug deposition are nozzle diameter, spray cone angle, swirl effects and break-up length. The diameter at the break-up length is important in terms of particle initialisation in the computational model as the particles need to be defined at the break-up length rather than at a point source at the nozzle exit. This can be approximated by

$$d_{\mathrm{bul}} = 2(d_{\mathrm{n}} + L_{\mathrm{bu}} \tan \phi) \tag{9}$$

where d_{bul} is the diameter at the break-up length, ϕ is the half angle between the spray sheet and the spray centreline (Fig. 4a), L_{bu} is the break-up length and d_{n} is the nozzle diameter. However, this linear approximation does not take into account any momentum losses during the entire spray penetration and gives an over-prediction of the diameter as L_{bu} is further downstream. Because of sensitive information regarding corporate patents over the design of nasal spray devices, detailed information is not attainable to quantify some of the design parameters such as the nozzle diameter, pressure-swirl chambers and cone angles. By applying the camera magnification ratio 1 pixel: 3 μm to the images, and using imaging analysis software (Adobe Photoshop CS) measurements for the cone angle, nozzle diameter and break-up length were ascertained and are summarised in Table 2.

The 2D velocity field produced by the PIV system found that the exit velocity from the nozzle was approximately 15 m/s. The maximum velocity reached 17 m/s in the region around 0.1 m downstream. It should be noted that this value is a consequence of a continuous spray which induces a continuous momentum force applied to the bulk spray flow caused by the upstream pressure. For nasal spray applications where the upstream pressure is applied in a short instance, the continuous momentum does not exist. The development of the spray is therefore an unsteady characteristic which is beyond the scope of this investigation. The initial velocity however is more applicable as the atomisation near the nozzle is the same for a continuous spray as it is for a pulsed spray. This is due to the atomisation dependence on the hydraulics of the flow within the atomiser, which governs the emerging liquid stream and the final disintegration into droplets.

Table 2
Spray device parameters for investigation

Measured parameters	Value
Nozzle diameter	≈ 0.5 mm
Diameter at break-up length	≈ 4 mm
Spray cone angle	≈ 30°
Initial particle velocity	≈ 15 m/s
Break-up length	≈ 3.5 mm

These measured values along with the observed images from Fig. 4 enabled confidence in determining the appropriate parameters and setting a corresponding range of realistic values. The chosen parameters were the swirl fraction, particle size, spray cone angle and the spray diameter at break-up length as summarised in Table 3. The swirl fraction parameter was included as the amount of swirl exerted onto the particles can be controlled by the internal swirl chamber design of a pressure-swirl atomiser [29]. The swirl fraction sets the fraction of the velocity magnitude to go into the swirling component of the flow where the direction of the swirl component is defined using the right-hand rule about the axis (a negative value for the swirl fraction can be used to reverse the swirl direction).

The spray cone angle defines the degree of dispersion of the spray into the airway. Studies have shown that the spray angle

Table 3
Spray device parameters for investigation

Parameter for investigation	Values		
Swirl fraction	0.1 	0.5 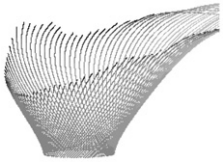	0.9 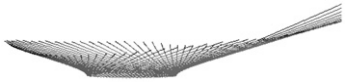
Particle size	10 μm 		20 μm 
Spray cone angle	20° 		60° 
Spray diameter at break-up length	2 mm 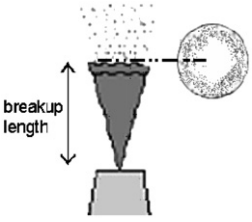		4 mm 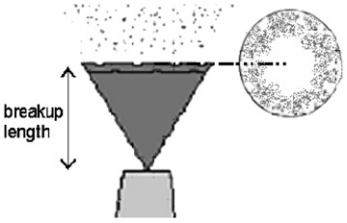

is influence by the nozzle dimensions, upstream pressure, liquid properties and the density of the medium into which the liquid is sprayed [30,31]. Its effect on particle deposition has been previously discussed by the authors in [2] where it was found that a wider spray cone angle dispersed more particles further towards the walls. This increases deposition of smaller particles as the particles are projected into streamlines that exist closer to the walls. For the numerical simulation, mono-sized particles were released as a hollow spray cone from the centre location of the each nostril. The spray cone angle was fixed at 40° and the distance of the release location from the nostril inlet was approximately 3 mm which assumes that the nasal spray device is actuated at the inlet. Different locations as well as different insertion angles and spray cone angles have previously been discussed by the authors in [2] and this variable was made constant by using the one location with a vertical insertion orientation.

3.2. Validation by particle deposition efficiency

In particle deposition studies, the Stokes number (St) given by

$$St = \frac{\rho_p d_p^2}{18\mu_g}\frac{U}{D} \tag{10}$$

is a ratio of the relaxation time

$$\tau = \frac{\rho_p d_p^2}{18\mu_g} \tag{11}$$

to the particle's characteristic time D/U, where U is the air phase system characteristic velocity normally taken as the air phase inlet value and D is the characteristic length. The Stokes number is a measure of the influence of the inertial effects during a particle's trajectory. However, its application to nasal cavity geometries does not give a fair representation as the characteristic length, D, and flow rate changes dynamically due to sharp changes in the nasal cavity geometry. Another parameter used for normalizing impaction-dominant deposition studies is the inertial parameter, I, given by

$$I = Qd_{ae}^2 \tag{12}$$

where Q is the airflow rate. It is a convenient parameter that compares deposition against different flow rates and particle sizes at aerodynamic diameters, although it also has drawbacks in its use of a constant flow rate which does not take into account the airway geometry. Despite its drawbacks it is widely used for presenting particle deposition efficiencies, especially for *in vivo* data, where it is difficult to determine an adequate characteristic length for realistic human airways.

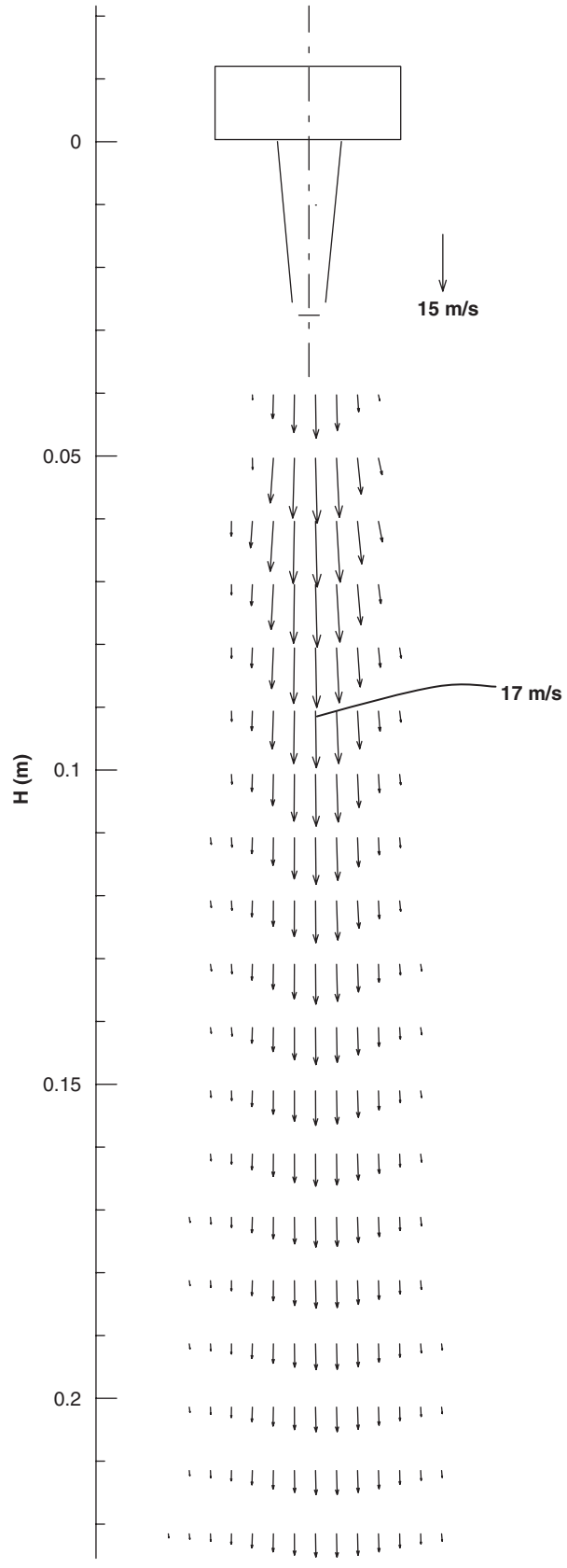

Fig. 5. PIV 2D vector plot of the averaged mean droplet velocity field of the spray nozzle.

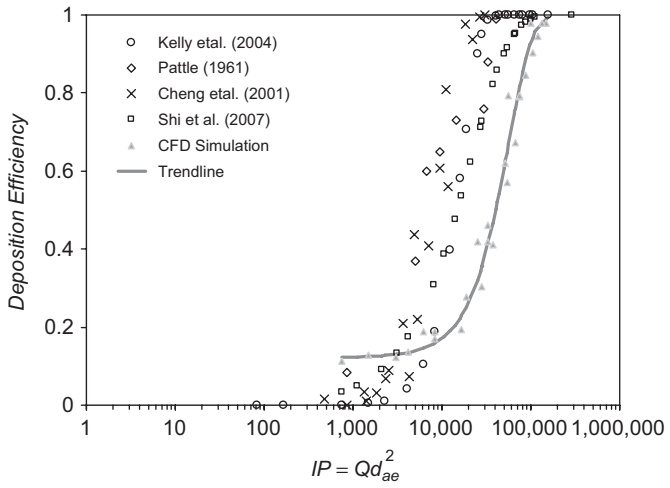

Fig. 6. CFD simulation results for total deposition of particles against inertial parameter compared with the experimental data.

Monodispersed particles in the range of 1–30 μm were released passively into the nasal cavity with flow rates of 5, 7.5, 10 and 15 L/min. The deposition of particles as a function of the inertial parameter is shown in Fig. 5 which displays the characteristic curve associated with inertial deposition. The results from the simulation are compared with the empirical equation

$$\eta = 1 - \exp(-(5.86E - 0.5 \cdot d_{\mathrm{ae}}^2 Q)^{2.1892}) \quad (13)$$

obtained by Kelly et al. [3] experimental studies using a nasal replica dubbed the Viper model. Differences in deposition may be attributed to the inter-subject variability between the nasal cavity models obtained by Kelly et al. [3] (53-year-old Caucasian male) with the model used in the present study (25-year-old Asian male), while Häußerman et al. [32] also states that nasal cavity replicate casts with wider airways can cause less deposition due to secondary flow. Furthermore, Kelly et al. [3] points out that differences in comparison of particle inertial deposition with different models can be explained by inertial impaction considerations. For $d_{\mathrm{ae}}^2 Q$ values less than $2000\,\mu m^2\,cm^3/s$ particles have a short relaxation time, which allows the particles to adjust to flow streamlines and hence the effect of different geometries is less significant. Accordingly, the comparison between the deposition curve of the CFD simulation and the experimental data [12] is fairly similar. As the value of $d_{\mathrm{ae}}^2 Q$ increases the particles relaxation time increases and the particles are more likely to continue a linear trajectory that deviates from a curving streamline. The differences in geometries that cause curvatures in streamlines are therefore significant for larger inertial particles (Fig. 6).

3.3. Velocity flow field

The flow field in the right nasal cavity was investigated at a flow rate of 10 L/min. Streamlines passing through four cross-sections labelled from A–A' through to D–D' alphabetically within the nasal cavity are shown in Fig. 7a. Air enters the nostril inlet at a velocity of 1 m/s before encountering a 90°

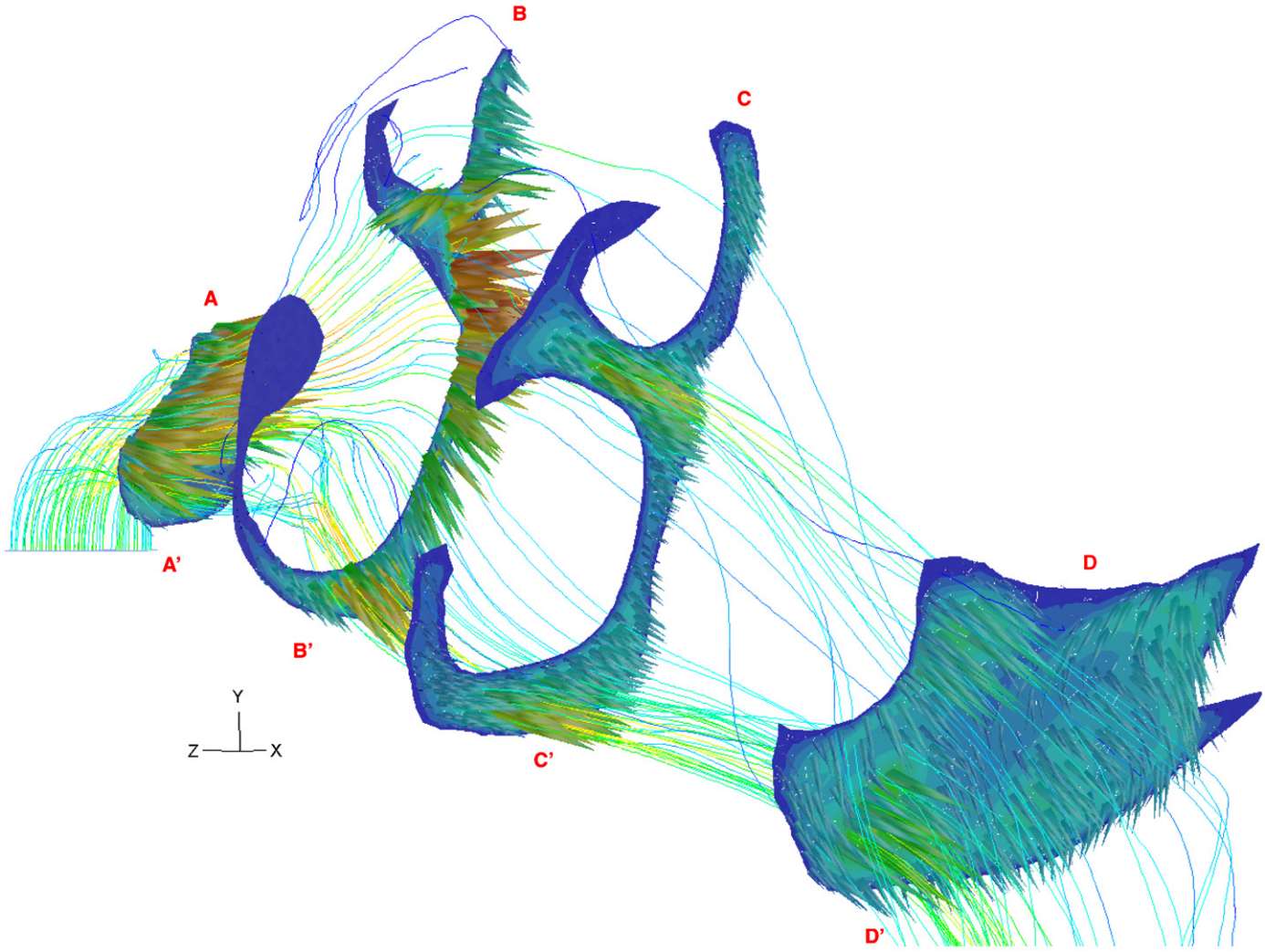

Fig. 7. Airflow streamlines passing through velocity contours taken at different coronal sections in the right nasal cavity.

curve. The air then accelerates as it squeezes through a narrowing region called the nasal valve and a maximum velocity of 2.18 m/s is reached in this region (Section A–A'). This acceleration and high velocity region will enhance a particles' impactability. Beyond the nasal valve the nasal airway expands and the air experiences a large deceleration. Regions of recirculation are found in the upper regions of the cavity known as the olfactory region. The streamlines separate into three main regions of flow with the majority passing through the middle airway and along the floor of the airway in the septum side of the nasal cavity. A smaller proportion of air passes through the upper region of the airway (Section C–C'). This division of air after the nasal valve expansion is also seen in Hahn et al. [23] where it was found that ≈ 50% of the inspired air flowed through the combined middle and inferior airway while ≈ 14% through the upper olfactory region. Similarly, simulations by Zamankhan et al. [14] and Subramanian et al. [25] also noted similar flow paths as well as regions of recirculation. At the nasopharynx (Section D–D') the left and right cavities have merged into one enlarged conduit where the airflow from both cavities merge and intense mixing occurs.

3.4. *Swirl fraction* (λ)

The swirl fraction sets the fraction of the velocity magnitude to go into the swirling component of the flow; thus, a higher fraction will produce a greater tangential velocity component. This increases the time taken to travel a given axial distance as the particle is swirling more and its residence time is longer. Additionally, the induced drag from the cross-flow of air helps to reduce the initially high momentum of the particle and the chances of particles travelling through the frontal regions of the nasal cavity increases. Fig. 8 shows high deposition of particles occurring in the frontal regions (Regions 1–3). The amount of swirl has a different effect for the two different particle sizes. For 10 μm particles with $\lambda=0.9$ deposition in the frontal zones increases, while for $\lambda=0.5$, a higher percentage of particles escape. Conversely for 20 μm particles, an increase in the swirl fraction decreases the deposition in the frontal zones. Some deposition in the middle zones occurs and 2.2% escape when $\lambda=0.9$. The reason for these localised deposition patterns can be better understood by observing the particle trajectories (Fig. 9). It is known that larger particles that possess high inertia

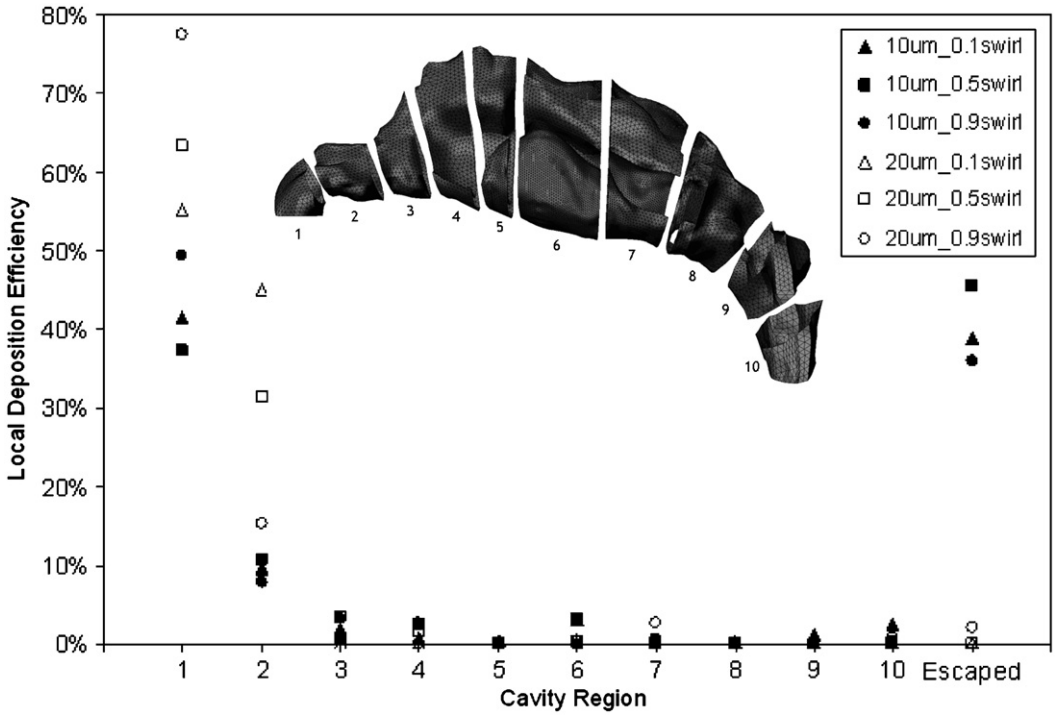

Fig. 8. Particle deposition within different sections of the nasal cavity. Sections 1–3 are the frontal region, Sections 4–7 are the middle region and Sections 8–10 are the posterior region.

(i.e. Stokes number characteristics) need to be aligned with the flow streamlines to avoid impaction. This implies that the particles need to be projected at a clear unobstructed path in the nasal airway rather than be projected at walls.

When $\lambda \to 0$, the velocity magnitude is entirely composed of an axial velocity, which projects the particles vertically. High inertia particles are projected directly at the roof of the nasal vestibule and do not have enough time to slow down, let alone adapt to the gas phase streamlines. However, smaller inertia particles can adapt to the flow streamlines more readily. One idea to overcome this was discussed by Inthavong et al. [2] which was to insert the nasal spray at an angle (insertion angle) that would provide such alignments with the flow streamlines. However, this technique is dependent on the user upon the application of the nasal spray device as well as the precise location of the nozzle.

When $\lambda \to 1$, the velocity magnitude is entirely composed of a tangential velocity and the particles are projected at a perpendicular direction to the nasal spray insertion angle. For 10 μm particles, deposition increases in the frontal zones as more particles are pushed towards the wall. For 20 μm particles this is also the case; however, instead of impaction into the upper roof when $\lambda = 0.1$, impaction is on the side walls. The horizontal projection of a small proportion of particles is then enhanced by the gas phase velocity which carries the particles along the floor of the nasal cavity. Without any obstructions to the flow, the particles are transported through to the nasopharynx area. A small increase in deposition within the middle and anterior regions is observed. At the nasopharynx, the flow changes direction at 90° which acts as another filter to capture high inertia particles that impact at the back. Although a swirl fraction of 1 is extreme and difficult to create within the atomiser design, its use in the present investigation provides a deeper understanding of the effects of the swirl fraction. The particle trajectories demonstrate that the swirling motion decreases the particles' initially high inertia due to the difference in the air and particle velocities.

3.5. Spray diameter at break-up length

The diameter of the spray cone at the break-up length can be controlled by the design of the atomiser. For example, the spray formation having a shorter/longer break-up length would produce a smaller/larger diameter at break-up. Additionally, the design of the nozzle diameter and spray cone angle produced from the nozzle has an effect on the spray diameter at break-up. For 10 μm particles, a larger diameter is shown to increase deposition in the frontal sections (Fig. 9a). As a result deposition in the middle and sections decreases as well as the number of particles escaping which is brought about by the initialized particles existing closer to the walls. This effect is similar to the spray cone angle effects where particles are projected outwards. Therefore, a design that couples a wide spray cone angle with a large spray diameter at break-up would bring about high frontal deposition. For 20 μm particles, the high inertial properties of the particle dominate the effect of the diameter at the break-up length and negligible change occurs (Fig. 10b).

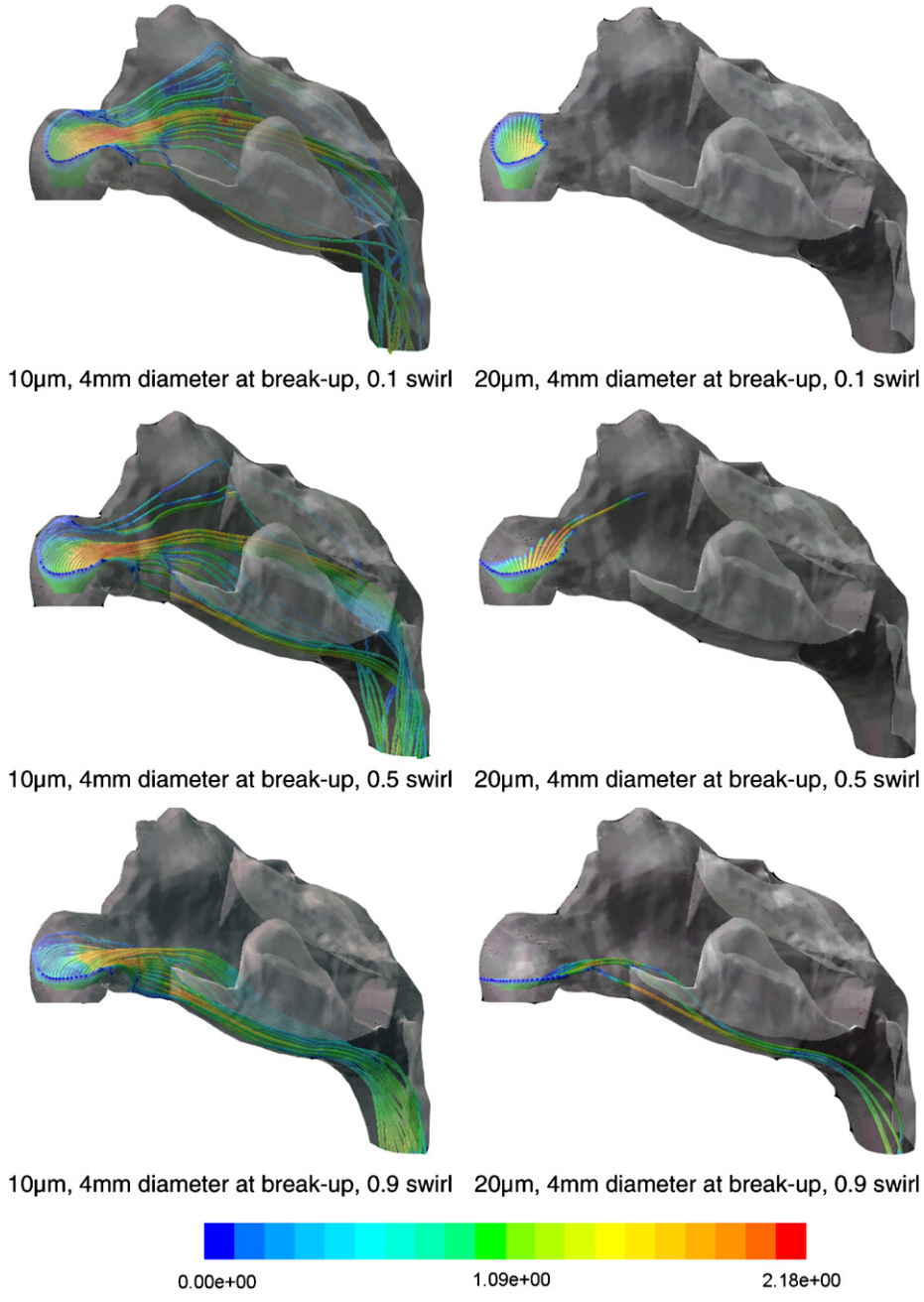

Fig. 9. Particle trajectories for 10 and 20 μm particles at different swirl fractions.

3.6. Implications for nasal drug delivery

The results from this study were aimed at gaining a greater insight into what parameters are important in the design of nasal drug delivery devices. The results revealed high deposition occurring in the frontal regions of the nasal cavity. It is well recognized that one of the functions of the nose is to filter out foreign particulates during inhalation, which was mainly thought to be attributed to cilia (nasal hairs) movement within the nose. However, the filtering function also extends to the airway geometry at multiple locations in the nasal cavity. In the frontal sections, Regions 1 and 2, the flow experiences a curvature in the streamlines which acts similar to inertial impactors that filter out high inertial, large particles. Another filter is the contraction of the nasal airway into the smallest cross-sectional area; the nasal valve region where particles are accelerated increasing their inertial property. Finally, another 90° bend exists at the nasopharynx which acts as a final filter before particles enter the lower airways. This may be one explanation for why patients experience an undesirable 'taste' after taking drugs via the nasal cavity after patients continually sniff the drug further in.

The filtering curvature in the frontal sections along with the constricting nasal valve region is most significant for therapeutic drug delivery as it prohibits larger particles to penetrate into

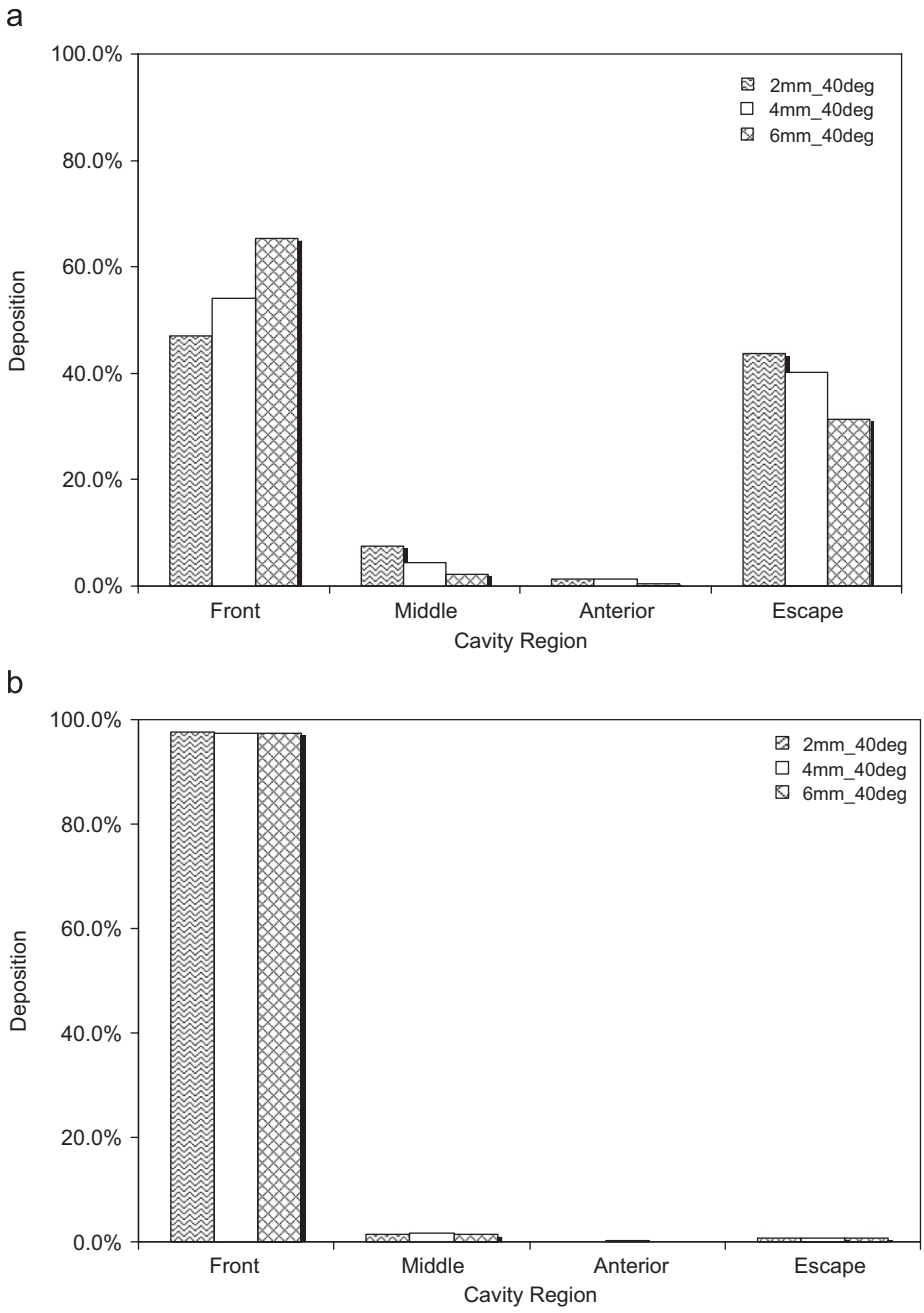

Fig. 10. (a) Regional deposition of 10 μm particles released at different spray cone diameters. (b) Regional deposition of 20 μm particles released at different spray cone diameters.

the middle cavity region for deposition onto the highly vascularised mucosal walls. One possible solution is to instruct users to insert the spray deeper or to develop spray devices that will naturally be inserted deeper with particles being released beyond the frontal curvature. The swirl fraction was used to create a vortical flow for the particles. It was found that high swirl fractions cause the particles to travel tangentially and that the spray penetration in the axial distance is very flat. This altered the particle trajectories since the particles reach equilibrium with the airflow field in different locations and hence different flow streamlines, which produces different local deposition sites. This effect is significant for 10 and 20 μm particles that exhibit low and high inertial particles. In practical terms, such an extreme swirl fraction may not be possible without the production of a wide spray cone angle in the design of the internal spray and optimisation studies would be required in the design process.

4. Conclusion

This study obtained experimental images of a continuous spray formation from a nasal spray device in order to determine which parameters were important for studies into the design of effective nasal drug delivery devices. It was found that there

Table 4
Particle deposition in different regions of nasal cavity

Particle (μm)	Swirl fraction	Front (%)	Middle (%)	Anterior (%)	Escape (%)
10	0.1	53.8	3.6	3.8	38.8
	0.5	51.2	3.1	0.2	45.6
	0.9	63.2	0.6	0.2	36.0
20	0.1	100.0	0.0	0.0	0.0
	0.5	98.3	1.7	0.0	0.0
	0.9	93.8	3.1	0.9	2.2

was a break-up length from the nozzle which is caused by the internal atomiser of the nasal spray. Particles were formed at this break-up length at a cone diameter greater than the spray nozzle diameter. It was found that a larger diameter at the break-up length led to an increase in particle deposition in the frontal sections of the nasal cavity (Table 4). The swirl fraction determined how much of the velocity magnitude went into a tangential component. The effect of the swirl fraction differed for 10 and 20 μm particles since the particles were severely altered by the swirl fraction and hence local deposition sites are altered. By combining a swirling component along with a narrow spray into the main streamlines, greater penetration of larger particles into the nasal cavity may be possible. Therefore, the results from this qualitative study aimed to assist the pharmaceutical industry to improve and help guide the design of nasal spray devices such as the manipulation of the swirl fraction parameter which will impart vortical flow on the particles.

5. Summary

This study obtained experimental images of a continuous spray formation from a nasal spray device in order to determine what parameters were important for studies into the design of effective nasal drug delivery devices. An experimental test rig complete with PIV and PDIA laser visualisation systems was constructed to identify what parameters were pertinent to nasal spray applications. Experimental images of particle formation from a nasal spray device were taken to determine critical parameters for the study and design of effective nasal drug delivery devices. The external parameters that were found to be significant for nasal spray drug delivery were: particle size, diameter of spray cone at a break-up length and a spray cone angle. The establishment of these parameters through imaging analysis allowed appropriate values to be ascertained which were then transposed into initial particle boundary conditions for numerical analysis.

The computational fluid dynamics Eulerian–Lagrangian scheme was utilized to track mono-dispersed particles (10 and 20 μm) at a breathing rate of 10 L/min. One parameter, the break-up length from the nozzle which is caused by the internal atomiser of the nasal spray, showed that the particles were formed at this break-up length at a cone diameter greater than the spray nozzle diameter rather than from a point source. It was found that a larger diameter at the break-up length led to an increase in particle deposition in the frontal sections of the nasal cavity. The swirl fraction determined how much of the velocity magnitude went into a tangential component. The effect of the swirl fraction differed for 10 and 20 μm particles since the particles were severely altered by the swirl fraction and hence local deposition sites are altered. By combining a swirling component along with a narrow spray into the main streamlines, greater penetration of larger particles into the nasal cavity may be possible. Therefore, the swirl fraction parameter presents an opportunity for design engineers to come up with novel designs that will impart vortical flow on the particles. The results from this study aimed at providing an insight to assist the pharmaceutical industry to improve and help guide the design of nasal spray devices.

Acknowledgements

The financial support provided by the Australian Research Council (project ID LP0347399 and LP0561870) is gratefully acknowledged.

Conflict of interest statement

All the authors declare that there is no potential conflict of interest including any financial, personal or other relationships with other people or organisations within that could inappropriately influence (bias) this work. The paper is an original research article that was financially supported by the Australian Research Council (project ID LP0347399 and LP0561870).

References

[1] J. Kimbell, J.D. Shroeter, B. Asgharian, B.A. Wong, R.A. Segal, C.J. Dickens, et al., Optimisation of nasal delivery devices using computational models, Res. Drug Del. 9 (2004) 233–238.
[2] K. Inthavong, Z.F. Tian, H.F. Li, J.Y. Tu, W. Yang, C.L. Xue, et al., A numerical study of spray particle deposition in a human nasal cavity, Aerosol Sci. Technol. 40 (2006) 1034–1045.
[3] J.T. Kelly, B. Asgharian, J.S. Kimbell, B.A. Wong, Particle deposition in human nasal airway replicas manufactured by different methods. Part 1: inertial regime particles, Aerosol Sci. Tech. 38 (2004) 1063–1071.
[4] G.J. Zwartz, R.A. Guilmette, Effect of flow rate on particle deposition in a replica of a human nasal airway, Inhal. Toxic. 13 (2001) 109–127.
[5] J. Gao, D. Jiang, Z. Huang, X. Wane, Experimental and numerical study of high-pressure-swirl injector sprays in a direct injection gasoline engine, Proc. Inst. Mech. Eng. A J. Power Energy 219 (8) (2005) 617–629.
[6] J. Straatsma, G. Van Houwelingen, A.E. Steenbergen, P. De Jong, Spray drying of food products: 1. Simulation model, J. Food Eng. 42 (2) (1999) 67–72.
[7] J. Kesavanathan, R. Bascom, D.L. Swift, The effect of nasal passage characteristics on particle deposition, J. Aerosol. Med. 11 (1998) 27–39.
[8] S.P. Newman, F. Moren, S.W. Clarke, Deposition pattern of nasal sprays in man, Rhinology 26 (1998) 111–120.
[9] D.L. Swift, Inspiratory inertial deposition of aerosols in human nasal airway replicate casts: implication for the proposed NCRP lung model, Radiat. Prot. Dosim. 38 (1991) 29–34.
[10] Y.S. Cheng, T.D. Holmes, J. Gao, R.A. Guilmette, S. Li, Y. Surakitbanharn, et al., Characterization of nasal spray pumps and deposition pattern in a replica of the human nasal airway, J. Aerosol. Med. 14 (2) (2001) 267–280.

[11] J.D. Suman, B.L. Laube, T.C. Lin, G. Brouet, R. Dalby, Validity of *in vitro* tests on aqueous spray pumps as surrogates for nasal deposition, Pharma. Res. 19 (2002) 1–6.
[12] I. Hörschler, M. Meinke, W. Schröder, Numerical simulation of the flow field in a model of the nasal cavity, Comp. Fluids 32 (2003) 39–45.
[13] J.Y. Tu, B. Abu-Hijleh, C. Xue, C.G. Li, CFD simulation of air/particle flow in the human nasal cavity, in: Proceedings of 5th International Conference on Multiphase Flow, Yokohama, Japan, 2004.
[14] P. Zamankhan, G. Ahmadi, Z. Wang, P.H. Hopke, Y.S. Cheng, W.C. Su, et al., Airflow and deposition of nanoparticles in a human nasal cavity, Aerosol Sci. Technol. 40 (2006) 463–476.
[15] Y. Zhang, W.H. Finlay, E.A. Matida, Particle deposition measurements and numerical simulation in a highly idealized mouth-throat, J. Aerosol Sci. 35 (2004) 789–803.
[16] D. Isabey, H.K. Chang, Steady and unsteady pressure-flow relationships in central airways, J. Appl. Physiol. 51 (1981) 1338–1348.
[17] H. Shi, C. Kleinstreuer, Z. Zhang, Laminar airflow and nanoparticle or vapor deposition in a human nasal cavity model, J. Biomech. Eng. 128 (2006) 697–706.
[18] S. Schreck, K.J. Sullivan, C.M. Ho, H.K. Chang, Correlations between flow resistance and geometry in a model of the human nose, J. Appl. Physiol. 75 (4) (1993) 1767–1775.
[19] K. Keyhani, P.W. Scherer, M.M. Mozell, Numerical simulation of airflow in the human nasal cavity, J. Biomech. Eng. 117 (1995) 429–441.
[20] J.P. Corey, A. Gungor, R. Nelson, J. Fredberg, V. Lai, A comparison of the nasal cross-sectional areas and volumes obtained with acoustic rhinometry and magnetic resonance imaging, Otolaryngol. Head Neck Surg. 117 (4) (1997) 349–354.
[21] O. Hilberg, F.T. Jensen, O.F. Pedersen, Nasal airway geometry: comparison between acoustic reflections and magnetic resonance scanning, J. Appl. Physiol. 75 (1993) 2811–2819.
[22] D.L. Swift, D.F. Proctor, Access of air to the respiratory tract, in: J.D. Brain, D.F. Proctor, L.M. Reid (Eds.), Respiratory Defence Mechanisms, Marcel Dekker, New York, NY, 1977, pp. 63–93.
[23] I. Hahn, P.W. Scherer, M.M. Mozell, Velocity profiles measured for airflow through a large-scale model of the human nasal cavity, J. Appl. Physiol. 75 (5) (1993) 2273–2287.
[24] M.H.D. Finck, I. Wlokas, Simulation of nasal flow by lattice Boltzmann methods, Comp. Biol. Med. 2006. doi:10.1016/j.compbiomed.2006.06.013.
[25] R.P. Subramaniam, R.B. Richardson, K.T. Morgan, J.S. Kimbell, R.A. Guilmette, Computational fluid dynamics simulations of inspiratory airflow in the human nose and nasopharynx, Inhal. Toxicol. 10 (1998) 91–120.
[26] H.K. Chang, Flow dynamics in the respiratory tract, in: H.K. Chang, M. Paiva (Eds.), Respiratory Physiology, an Analytical Approach, Dekker, New York, 1989, pp. 54–138.
[27] K.J. Sullivan, H.K. Chang, Steady and oscillatory trans-nasal pressure-flow relationships in healthy adults, J. Appl. Physiol. 71 (1991) 983–992.
[28] C.T. Crowe, M. Sommerfeld, Y. Tsuji, Multiphase Flows with Droplets and Particles, CRC Press, Boca Raton, FL, 1998.
[29] A.H. Lefebvre, Atomization and Sprays, Hemisphere Publishing Corporation, 1989.
[30] K.R. Babu, M.V. Narasimhan, K. Narayanaswamy, Correlations for prediction of discharge rate, cone angle and aircore diameter of swirl spray atomisers, in: Proceedings of the 2nd International Conference on Liquid Atomisation and Spray Systems, Madison, WI, 1982, pp. 91–97.
[31] N.K. Rizk, A.H. Lefebvre, Internal flow characteristics of simplex swirl atomisers, AIAA J. Propul. Power 1 (3) (1985) 193–199.
[32] S. Häußermann, A.G. Bailey, M.R. Bailey, G. Etherington, M.J. Youngman, The influence of breathing patterns on particle deposition in a nasal replicate cast, J. Aerosol. Sci. 33 (2001) 923–933.

Kiao Inthavong was born in Vientiane, Laos, in 1979. He received a Bachelor's Degree in Mechanical Engineering from Swinburne University, Australia, in 2003 and is currently a PhD candidate at RMIT studying gas-particle flows in the nasal cavity. His research interests include heat transfer, computational fluid dynamics (CFD), numerical heat transfer, multiphase flows and biomedical applications.

Zhaofeng Tian was born in Taiyuan, China, in 1975. He received a Bachelor's Degree from Shanghai Jiaotong University, China, in 1997 and a Master's Degree from the University of New South Wales, Australia, in 2002. Since 2003, he has been with the RMIT University, Australia, where he attained his PhD in Mechanical Engineering. His research interests focus on numerical simulation of two-phase flow and its engineering applications.

Jiyuan Tu was born in Ningbo, China, in 1958. He received a Bachelor's Degree from Northeast University, China, in 1982, a Masters Degree from the same university and a PhD from Royal Institute of Technology, Stockholm in 1992. Then he worked with the University of NSW as a research fellow and Australian Nuclear Science and Technology Organisation (ANSTO) as a senior research scientist and is currently a Professor at the RMIT University in the School of Aerospace, Mechanical and Manufacturing Engineering. His research interests focus on computational fluid dynamics (CFD), numerical heat transfer, multiphase flows and biomedical applications.

William Yang was born in Shanghai, China, in 1963. He completed a Bachelor of Engineering in Mechanical Engineering at Tongji University, Shanghai, China, in 1985. Then he was educated at Swinburne University of Technology, Melbourne, Australia, where he received a Master of Engineering and a Doctor of Philosophy in Mechanical Engineering. Prior to joining CSIRO in 2003, Yang lectured with the School of Mechanical and Manufacturing Engineering at Swinburne University of Technology for seven years. Currently he is a senior research scientist with CSIRO Minerals, Melbourne, Australia. Yang has substantial research experience in both mechanical and biomechanical engineering area and has extensive knowledge of fluid flow measurement techniques such as hot-wire, laser Doppler anemometry (LDA) and particle image velocimetry (PIV) systems.